INSTITUTE OF PHYSICS PUBLISHING JOURNAL OF PHYSICS B: ATOMIC, MOLECULAR AND OPTICAL PHYSICS

J. Phys. B: At. Mol. Opt. Phys. **34** (2001) 2807–2821 www.iop.org/Journals/jb PII: S0953-4075(01)20321-6

Electron collisions with Cl_2O using the R-matrix method

K L Baluja[1], **N J Mason, L A Morgan and Jonathan Tennyson**

Department of Physics and Astronomy, University College London, Gower Street, London WC1E 6BT, UK

Received 27 December 2000, in final form 31 May 2001

Abstract

The R-matrix method is used to calculate the elastic and excitation cross sections of seven low-lying electronically excited states of the Cl_2O molecule. Sixteen states consisting of eight singlets and eight triplets are included in the close-coupled expansion. These states have vertical excitation energies in the range 3.17–8.75 eV, which are in fair agreement with other more sophisticated calculations. We find an electronically bound, but probably dissociative, state of Cl_2O^- with $^2A_1$ symmetry with an adiabatic electron affinity of 0.4423 eV at the equilibrium geometry of Cl_2O. There is a shape dissociative resonance of $^2B_2$ symmetry at 2.096 eV. We also find core-excited shape resonances in $^2A_1$, $^2A_2$, $^2B_1$ and $^2B_2$ symmetries. Cross sections are obtained for rotationally elastic and electronically inelastic scattering for electron impact energies up to 10 eV. Anionic and neutral dissociation products are considered.

(Some figures in this article are in colour only in the electronic version)

1. Introduction

The study of the chlorine oxides is an active area of research due to the involvement of these molecules in photochemical transformations that lead to ozone depletion in the Earth's stratosphere. However, the interaction of electrons with these molecules remains poorly characterized. In a previous letter (Baluja *et al* 2000), we reported spectroscopic and electron impact scattering calculations for the ClO molecule, which is central to the catalytic loss process of ozone depletion in the stratosphere. In the present paper we extend this study to the Cl_2O molecule. Although the Cl_2O molecule is not present in significant quantities in the stratosphere, its study is expected to aid in the understanding of atmospheric processes, because it is structurally related to other, larger, chlorine oxides which play a more prominent role.

[1] Permanent address: Department of Physics and Astrophysics, University of Delhi, Delhi 110007, India.

Experimental work on Cl_xO_y molecules is difficult because they are highly reactive and unstable, and therefore have to be synthesized *in situ*. Most of the earlier experimental work on Cl_2O has been spectroscopic. Its absorption spectrum in the visible and ultraviolet regions (2–6.5 eV) was measured by Goodeve and Wallace (1930), Finkelnburg *et al* (1931), Lin (1976), Molina and Molina (1978) and Knauth *et al* (1979). In this energy range there are three absorption bands related to the excitation of valence electronic states, each with dissociative character (Nickolaisen *et al* 1996). This energy range has been extended by Nee (1991) and Motte-Tollet *et al* (1997, 1998).

Experimental studies on electron collisions with Cl_xO_y molecules have been restricted to studies on OClO (Senn *et al* 1999, Field *et al* 2000). However, recently one of us (NJM, see Sailer *et al* 2001) has commenced experimental work on Cl_2O; this work will be discussed below.

The open-shell nature of many of the Cl_xO_y compounds makes them difficult systems to treat theoretically. Even though Cl_2O is a closed-shell molecule, it is electron-rich and there are many low-lying electronic states. Electron correlation must therefore be taken into account to characterize these states properly.

In this paper we report the first electron collision calculations on the ClOCl isomer of Cl_2O. These calculations are performed using the UK polyatomic R-matrix code (Morgan *et al* 1997, 1998), taking particular advantage of this method to give a good representation of the electron correlation in several excited states of the molecule (Tennyson 1996a).

2. Method

2.1. General considerations

The basic idea of the R-matrix method is the division of configuration space into two regions, an inner region and an outer region (Burke and Berrington 1993). In the inner region, here defined by a sphere of radius 10 a_0 centred at the Cl_2O centre of mass, the wavefunction for a fixed geometry is written using the configuration interaction (CI) expression

$$\Psi_k = \mathcal{A} \sum_{ij} a_{ijk} \phi_i^N \eta_{ij} + \sum_j b_{jk} \phi_j^{N+1} \tag{1}$$

where ϕ_i^N represents the ith state of the N-electron target, η_{ij} is a function representing the continuum electron and $\mathcal{A}$ is an anti-symmetrization operator. Coefficients a_{ijk} and b_{jk} are variational parameters determined as a result of the matrix diagonalization. The continuum functions are the only functions with amplitude on the R-matrix boundary. The second sum in (1) comprises configurations composed of short-range functions ϕ_j^{N+1} which are multi-centred quadratically integrable (L^2) functions constructed from the target occupied and virtual orbitals. To obtain reliable results it is important that a balance between the N-electron target representation and the $(N + 1)$-electron collision complex representation be properly maintained. The choice of appropriate ϕ_j^{N+1} is crucial in this (Tennyson 1996b). Thus, for example, the static-exchange model is only well defined for SCF targets in this case when only one target state is included in the coupled-state expansion and only those (L^2) functions are included which correspond to the single excitations from occupied molecular orbitals. When this one-target state is represented by a CI wavefunction we define the scattering model as a 'reduced one-state model' which is as close as it is possible for us to come to a static-exchange calculation while using a correlated target wavefunction.

Inside the R-matrix sphere, full electron–electron and exchange interactions are explicitly modelled. Outside the sphere, only long-range multipolar interactions between the scattering electron and the various target states are included. Cl_2O is a dipolar system which has to be

taken into account both by propagating the R-matrix to large distance, 50 a_0 in this paper, and by considering convergence with respect to the partial wave expansion used for the continuum orbitals, η_{ij}.

2.2. Target states

Microwave spectroscopy (Herberich *et al* 1966, Nakata *et al* 1981) and electron diffraction experiments (Dunitz and Hedberg 1950, Bru *et al* 1952) have shown that the Cl_2O molecule is bent and belongs to the C_{2v} symmetry group. According to the microwave study of Nakata *et al* (1981), the Cl–O bond length is 1.695 87 Å and the angle ClOCl is 110.886° at equilibrium. This equilibrium geometry is used as the starting point for the present calculations, but variations about this geometry were also studied.

There are three sets of theoretical calculations for the vertical excitation energies of the ClOCl molecule. Del Bene *et al* (1995) calculated the vertical excitation energies of the singlet states only using the equation of motion coupled cluster method. Toniolo *et al* (2000) also presented an *ab initio* study of only the singlet states of the ClOCl molecule by simulating the electronic spectra by calculating the semiclassical absorption cross sections. Nickolaisen *et al* (1996) have calculated the vertical transition energies for singlet and triplet states of the ClOCl molecule at the experimental ground-state geometry.

The Cl_2O molecule is rich in electrons. Its electronic ground-state configuration has been established through photoelectron spectroscopy (Cornford *et al* 1971, Motte-Tollet *et al* 1998) and confirmed by theory. A number of theoretical calculations are available, including those of Nickolaisen *et al* (1996), Lee (1996) and Beltrán *et al* (1999). The calculations of Nickolaisen *et al* (1996), the only ones available for both singlet and triplet electronically excited states, were performed using the Dunning correlation-consistent polarized valence triple-zeta basis. This set gave a total number of 98 basis functions. They also performed electronic energy calculations with a smaller valence double-zeta basis (involving only 50 basis functions) but the results were found to differ only slightly. With the triple-zeta basis set they calculated the vertical transition energies for the following 16 states: 1^1A_1, 2^1A_1, 1^1B_1, 2^1B_1, 1^1B_2, 2^1B_2, 1^1A_2, 2^1A_2, 1^3A_1, 2^3A_1, 1^3B_1, 2^3B_1, 1^3B_2, 2^3B_2, 1^3A_2 and 2^3A_2; we consider the same 16 states here and have retained these state labels. Nickolaisen *et al* (1996) used different state-averaged orbitals for each space and spin symmetry. The option of using different sets of molecular orbitals for each target state is not available to us since equation (1) relies on the use of a single set of orbitals for the whole calculation.

Our calculations on Cl_2O used the double-zeta plus polarization Gaussian basis set of Dunning and Hay (1977) and Magnusson and Schaefer (1985). We used the SCF molecular orbitals of the ground state in our CI calculations of all the 16 states which are included in the scattering calculation. Our R-matrix calculations demand the same set of orbitals for all the states included in the expansion of the wavefunction of the electron–molecular scattering system, so our state energies are slightly higher than the electronic energies calculated by Nickolaisen *et al* (1996). We divided our calculation into 22 core electrons and 20 valence electrons. The core consists of all doubly occupied molecular orbitals filled up to $5a_1$, $1b_1$, $4b_2$ and $1a_2$ molecular orbitals. The complete active space (CAS) comprises 20 electrons in 12 molecular orbitals of type $6a_1$, $5b_2$, $7a_1$, $2b_1$, $6b_2$, $8a_1$, $2a_2$, $9a_1$, $7b_2$, $3b_1$, $10a_1$, and $8b_2$. For the ground state all molecular orbitals up to $3b_1$ are doubly occupied giving the state designation $X\ ^1A_1$. In our target state calculations, the Cl 1s, 2s and 2p electrons, along with O 1s electrons were frozen in their SCF orbitals. These 22 atomic electrons occupy 11 molecular orbitals: ($1a_1$, $1b_2$), $2a_1$, ($3a_1$, $2b_2$), ($4a_1$, $3b_2$), ($5a_1$, $4b_2$), ($1a_2$, $1b_1$). The pairs of molecular orbitals within the brackets are nearly degenerate. The last three pairs have almost the same

Table 1. Vertical energy excitations (in eV) for the Cl_2O target states generated using a CAS CI model at equilibrium geometry. Also given are the dominant configuration of each state, the number of configurations, N, in the CAS and the excitation values of Nickolaisen *et al* (1996).

			Vertical excitation	
State	Configuration	N	This work	Nickolaisen *et al*
$X\,^1A_1$		480	0	0
$1\,^3B_1$	$3b_1^{-1}10a_1$	524	3.17	2.63
$1\,^1B_1$	$3b_1^{-1}10a_1$	396	4.00	3.42
$1\,^3A_2$	$2a_2^{-1}10a_1$	529	4.50	4.04
$1\,^3B_2$	$7b_2^{-1}10a_1$	556	4.53	4.18
$1\,^3A_1$	$9a_1^{-1}10a_1$	536	4.69	4.40
$1\,^1B_2$	$7b_2^{-1}10a_1$	444	5.42	4.99
$1\,^1A_2$	$2a_2^{-1}10a_1$	396	5.50	4.97
$2\,^1A_1$	$9a_1^{-1}10a_1$	480	5.85	5.45
$2\,^3A_2$	$3b_1^{-1}8b_2$	529	6.29	5.63
$2\,^1A_2$	$3b_1^{-1}8b_2$	396	6.43	5.88
$2\,^3A_1$	$7b_2^{-1}8b_2$	536	6.92	6.44
$2\,^3B_2$	$9a_1^{-1}8b_2$	556	7.01	6.59
$2\,^3B_1$	$2a_2^{-1}8b_2$	524	7.21	6.67
$2\,^1B_1$	$2a_2^{-1}8b_2$	396	7.83	7.35
$2\,^1B_2$	$9a_1^{-1}8b_2$	444	8.75	7.98

binding energy differing by only 0.12 eV. All the molecular orbitals in the core are bound by at least 220 eV. Our SCF calculations indicate that the highest occupied molecular orbital is $3b_1$ with a binding energy of 12.11 eV. According to the Koopman theorem this energy is approximately equal to the first ionization potential of the Cl_2O molecule. This value is close to the experimental vertical value 11.02 eV obtained by studying the photoelectron spectrum of the Cl_2O molecule (Motte-Tollet *et al* 1998). The lowest unoccupied molecular orbital is $10a_1$ with energy +1.35 eV and the next unoccupied orbital is $8b_2$ with energy +3.93 eV. All the 15 excited electronic states included in our calculations arise due to the promotion of one electron from one of the four valence molecular orbitals $2a_2$, $9a_1$, $7b_2$ and $3b_1$ to either the unoccupied molecular orbital $10a_1$ or $8b_2$. These states are modelled by a CAS CI whose configurations can be written as ($6a_1$, $5b_2$, $7a_1$, $2b_1$, $6b_2$, $8a_1$, $2a_2$, $9a_1$, $7b_2$, $3b_1$, $10a_1$, $8b_2$)[20].

Table 1 compares vertical excitation energies for the states considered in our calculation. These are compared with the calculations of Nickolaisen *et al* (1996). As stated above, our model gives energies which are consistently higher than the Nickolaisen *et al* (1996) results due to the constraint imposed by our scattering model. Nickolaisen *et al* (1996) also studied the photodissociation of the Cl_2O molecule using broadband flash photolysis. The experimental spectrum showed five prominent features with four absorption peaks at 171 nm (7.24 eV), 254 nm (4.88 eV), 420 nm (2.9 eV) and 540 nm (2.3 eV) and a shoulder on the 254 nm peak at 300 nm (4.1 eV). They assigned the 7.24 eV peak with the $2\,^1B_1$ state and the peak at 4.88 eV with the $1\,^1B_2$ state. The remaining observed features could not be correlated well with their computed results. Our model gives the value 7.83 eV for the $2\,^1B_1$ state, and 5.42 eV for the $1\,^1B_2$ state. These values are within approximately 10% of their respective experimental values. The calculated excitation energies of the singlets obtained by Del Bene *et al* (1995) and by Toniolo *et al* (2000) are lower than the Nickolaisen *et al* (1996) results by 0.5–1 eV.

Our model gives a dipole moment of 0.3815 au and quadrupole moments $Q_0 = 1.2456$ au and $Q_2 = 2.5774$ au at the equilibrium geometry of the Cl_2O molecule. Our value of dipole

moment is in agreement with the value 0.3378 au obtained by McGrath *et al* (1990) using second-order Moller–Plesset perturbation theory. We know of no experimental determination of the dipole moment of ClOCl molecule. The slight difference of about 10% between the two dipole moments may be due to the fact that their equilibrium geometry is computed with a polarized split-valence 6-31G basis set (Hariharan and Pople 1973) which is a smaller basis set than the one employed in this paper.

2.3. Scattering model

Our final calculations used the 16 target states given in table 1 in the close-coupling expansion (1), although a variety of test calculations were performed with fewer states in this expansion. In particular, we performed reduced one-state, eight-state and 16-state calculations for doublet states with A_1, B_1, B_2 and A_2 symmetries. In all calculations, the continuum orbitals were represented by Gaussians centred at the molecule's centre of gravity; the orbitals of Sarpal *et al* (1996) were used. Test calculations were performed for continuum orbitals up to g ($l \leqslant 4$) partial waves and up to f ($l \leqslant 3$) partial waves; the two calculations showed only minor differences. All our final calculations are with continuum orbitals up to f partial waves. These continuum orbitals were orthogonalized to the target orbitals retained in the calculation and those with an overlap of less than 2×10^{-7} were removed (Morgan *et al* 1997).

Calculations, from reduced 1-state upwards, were performed to test the stability of our model and assign resonances. These calculations included some with hand-picked configurations which allowed us to give orbital designation to the resonances we found and to probe the cause of pseudo-resonances which are high-energy artifacts of any truncated coupled-channels calculation.

One advantage of the CAS CI target model employed here is that the ϕ_j^{N+1} functions, see (1), can be defined in a fashion which retains the balance of the calculation (Tennyson 1996b). All $N + 1$ electron configurations of the appropriate total symmetry given by $(\text{core})^{22}$ $(6a_1, 7a_1, 8a_1, 9a_1, 10a_1, 2b_1, 3b_1, 5b_2, 6b_2, 7b_2, 8b_2, 2a_2)^{21}$ were retained, where the notation means that 22 electrons are frozen in the core and 21 electrons are freely distributed among the molecular orbitals given within the bracket, constrained only by symmetry considerations.

3. Results

3.1. Anionic bound state

Superficially, Cl_2O and H_2O have similar closed-shell electronic structure. The dipole moment of Cl_2O is nearly half of the dipole moment value 0.7532 au of water (Morgan 1998). However, Cl_2O supports a much stronger bound anionic state than water. All our models (except reduced one-state) found a bound state of Cl_2O^- with $^2A_1$ symmetry. The energy of the state was determined using our bound-state detecting code BOUND (Sarpal *et al* 1991). Our best model gave Cl_2O an electron affinity of 0.4423 eV at the equilibrium geometry. This is in contrast to the value 0.078 eV (Morgan 1998) of the binding energy of the anion state of $^2A_1$ symmetry of water. For water, if rotational motion is also included (Crawford and Garrett 1977), the dipole potential seen by the extra electron will be modified and will weaken the anionic binding energy. This is not the case for Cl_2O; the strength of the binding will be sufficient for this state to remain. Variation of this state with geometry is considered below.

We also performed a standard bound-state quantum chemistry calculation on the anionic state of $^2A_1$ symmetry using the same orbitals and model employed for the scattering

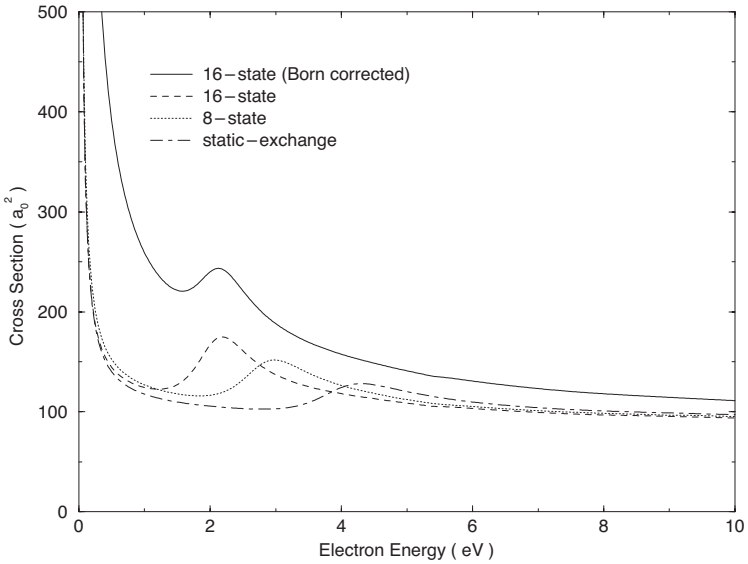

Figure 1. Elastic and rotational cross sections for electron impact on the X $^1A_1$ state of Cl_2O. Sixteen-state R-matrix elastic cross sections with $l \leqslant 3$: dashed curve; eight-state R-matrix elastic cross sections with $l \leqslant 3$: dotted curve; reduced one-state R-matrix elastic cross sections with $l \leqslant 3$: dot-dash curve; 16-state Born-corrected rotational cross section for the $J_K = 0_0 - 1_1$ transition: solid curve.

calculations. This calculation gave a very similar result: a Cl_2O electron affinity of 0.4434 eV at the equilibrium geometry.

3.2. Elastic scattering

We carried out the elastic scattering calculations in three models: reduced one-state, eight-state and 16-state. Our best model is the 16-state model, for which 64 channels are coupled for each scattering symmetry. The number of terms in the summation of equation (1) for each scattering symmetry is typically in the range 7800–7900. Due to the presence of long-range dipole interactions, the elastic cross section is formally divergent in the fixed-nuclei approximation. However, the elastic scattering data can be exploited to yield rotational cross sections.

Due to the strength of the permanent dipole moment of the Cl_2O molecule, a large number of partial waves must be taken into account to obtain converged results. States with partial wave $l \geqslant 3$ omitted from our calculations were allowed for by using the Born approximation (Gianturco and Jain 1986). The rotational constants were calculated for Cl_2O at the equilibrium geometry giving 1.4041, 0.1239 and 0.1139 cm^{-1}. The ClOCl molecule is an asymmetric top but has one moment of inertia considerably greater than either of the other two. The value of the asymmetry parameter $\kappa = (2B - A - C)/(A - C))$ is -0.9845, which is close to -1, and therefore to a good approximation, it may be treated as prolate symmetric top. In figure 1, we present rotational cross sections for the allowed transition ($J = 0$, $K = 0$–$J' = 1$, $K' = 0$) by dipole excitation, where J is the rotational angular momentum and K is the projection of J along the A axis.

For all models, our results are characterized by a sharp rise, proportional to E^{-1}, in the elastic scattering cross section at energies below 0.5 eV for each symmetry. This behaviour

has been noted previously for strongly dipolar molecules (Fabrikant 1977, Baluja *et al* 2000). Indeed, test calculations which set the Cl_2O ground-state dipole moment to zero in the outer region led to the disappearance of this threshold feature, but other resonances remain intact.

The main feature in the elastic cross section is the presence of a shape resonance in the $^2B_2$ symmetry, even though the main contribution to the cross section comes from $^2A_1$ symmetry which cannot provide the necessary centrifugal barrier to trap the scattering electron. The $^2B_2$ symmetry resonance appears in all the models studied here. Since the resonance feature is present even in the reduced one-state model, it must be a shape resonance. In the reduced one-state model it appears at 4.35 eV provided we use a CAS CI target wavefunction. As the number of states included in the calculation increases, the position of the resonance shifts to lower energy and becomes narrower. This is due to the increased polarization effects which pull the peak towards lower energy. For our eight-state model, the resonance is near 3 eV. For our final 16-state model, the eigenphase sums are fitted to a Breit–Wigner form to yield resonance parameters (Tennyson and Noble 1984). The position and width of this resonance are 2.096 and 0.971 eV respectively. By manipulating the active space it is possible to assign the configuration of the resonances. The configuration of this shape resonance is $\ldots 3b_1^2 8b_2\ ^2B_2$.

3.3. Inelastic cross sections

Figures 2 and 3 present electron impact electronic excitation cross sections from the ground state to the three singlet and four triplet excited states respectively. We first describe the cross sections for the singlet states and then the triplet states.

By optical (dipole) selection rules, all transitions from the ground state to singlet excited states are allowed except to the $^1A_2$ state. The cross section for exciting the first singlet, $^1B_1$, state is shown in figure 2(*a*). This is a dipole-allowed transition with a small transition moment 0.1176 au. To incorporate the effects of higher partial waves for optically allowed cross sections, we use a closure formula (Crawford and Dalgarno 1971) in order to get converged cross sections. This correction increases with increasing energy and is about 12% at 10 eV. The Born-corrected cross sections are shown for our best model. The cross sections display a small shoulder around 5.3 eV in both our models. This is due to a resonance peak in $^2A_2$ symmetry with position at 5.261 eV and width 0.550 eV. A resonance peak of the same symmetry also appeared in the case of excitation of the $^3B_1$ state, but at a slightly higher energy. The hump in the eight-state calculation around 8.5 eV is a pseudo-resonance, which arises due to the neglect of higher states in the calculation; it is wiped out in the 16-state calculation. The integrated cross section for exciting the $^1B_1$ state is higher than for the corresponding $^3B_1$ state because the excitation of $^3B_1$ state is a spin-forbidden transition from the ground state.

Figure 2(*b*) displays the cross sections for the excitation of the $^1B_2$ state. This is a dipole-allowed transition with a transition moment of 0.2050 au. The Born-corrected cross sections for the 16-state model are shown. The Born correction becomes noticeable beyond 7 eV and is almost 50% at 10 eV. The structure in the 16-state model arises in the $^2A_1$ symmetry positioned at 7.460 eV with a width of 0.591 eV. The maximum contribution comes from $^2B_2$ symmetry. The pseudo-resonance in the eight-state model is present in $^2B_2$ symmetry, it is absent in our best model.

The final singlet transition considered here is the excitation of the $^1A_2$ state. The cross section is shown in figure 2(*c*). This transition is not dipole allowed due to symmetry considerations. The $^2B_2$ symmetry pseudo-resonance present in the eight-state model is shifted to a lower energy in the 16-state model.

The first excited triplet state has symmetry $^3B_1$. The corresponding integrated cross section is shown in figure 3(a). The results of our eight-state calculations are also shown for comparison

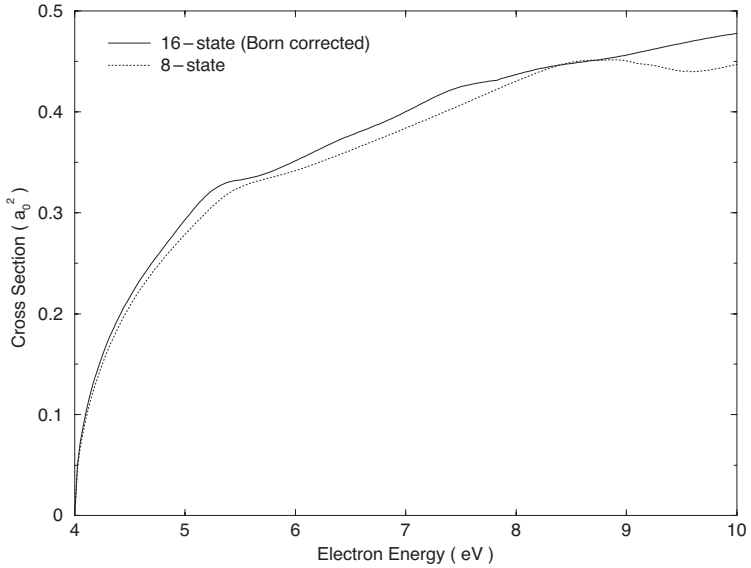

(*a*)

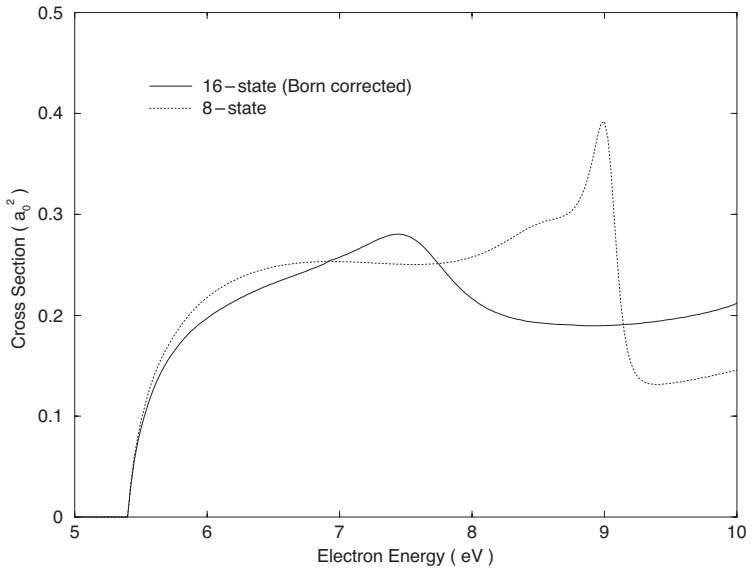

(*b*)

Figure 2. (*a*) Electron impact excitation of transition $X\,^1A_1$–$1\,^1B_1$ of Cl_2O. Solid curve: 16-state Born-corrected *R*-matrix cross sections; dotted curve: eight-state *R*-matrix cross sections. (*b*) Electron impact excitation of transition $X\,^1A_1$–$1\,^1B_2$ of Cl_2O. Solid curve: 16-state Born-corrected *R*-matrix cross sections; dotted curve: eight-state *R*-matrix cross sections. (*c*) Electron impact excitation of transition $X\,^1A_1$–$1\,^1A_2$ of Cl_2O. Solid curve: 16-state *R*-matrix cross sections; dotted curve: eight-state *R*-matrix cross sections.

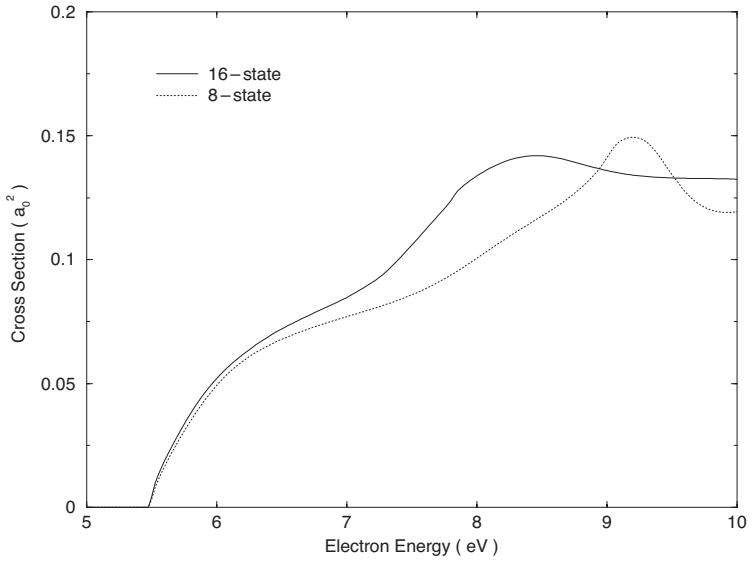

(*c*)

Figure 2. (Continued.)

with our 16-state calculation. We noticed three peaks in our eight-state calculation, in contrast to two peaks in the 16-state results. The peak at around 9 eV in the eight-state calculation arises in the $^2B_1$ symmetry and is a pseudo-resonance which is eliminated in the 16-state calculation. The first peak arises in the $^2B_1$ symmetry and the second weaker peak arises in the $^2A_2$ symmetry. The peaks in the 16-state calculations shift to lower energies and are narrower than the corresponding peaks in the eight-state results. The cross sections in our best model are lower in magnitude than our eight-state model due to the loss of flux into more accessible channels. The first resonance of the $^2B_1$ symmetry has resonance position 3.679 eV and width 0.202 eV, whereas the second broad peak of the $^2A_2$ symmetry is located at position 5.741 eV and has width 1.107 eV.

Figure 3(*b*) gives the excitation cross sections for the $^3A_2$ state. In the 16-state results, we notice two humps. The first hump is due to the combined effect of the resonances of the $^2B_2$ and $^2A_2$ symmetries, and the second hump is due to resonance of $^2B_1$ symmetry. The $^2B_2$ symmetry provides the dominant contribution to the integrated cross section. There is no structure in the $^2A_1$ symmetry but its contribution is more significant than the contributions of $^2B_1$ and $^2A_2$ symmetries. The resonance $^2B_2$ and $^2A_2$ symmetries have already been discussed. There is a peak in the $^2B_1$ symmetry around 7.53 eV which is also a resonance.

The excited states $^3A_2$ and $^3B_2$ are almost degenerate, differing only by 0.03 eV. Figure 3(*c*) shows our results for the excited state $^3B_2$. The only structure is in the prominent resonance of $^2B_2$ symmetry which appears at the same position as in the cross section results of the $^3A_2$ excited state. The contribution of $^2A_1$ symmetry is most significant beyond 6 eV. The contribution of $^2B_1$ and $^2A_2$ symmetries to the integrated cross section is negligible. The second peak in the eight-state calculation is smoothed out in the 16-state results.

The excitation cross sections for the $^3A_1$ state are shown in figure 3(*d*). This excitation process is almost completely dominated by the $^2A_1$ symmetry which has resonance parameters $E_r = 5.590$ eV and $\Gamma_r = 0.464$ eV. A very weak resonance structure in the $^2B_2$ symmetry around 5.4 eV is buried in the peak of $^2A_1$ symmetry. There is another peak in the $^2B_2$

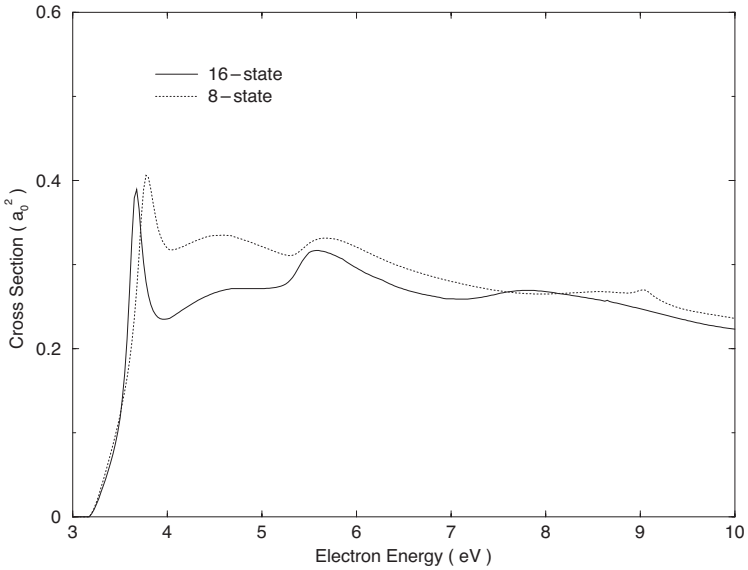

(*a*)

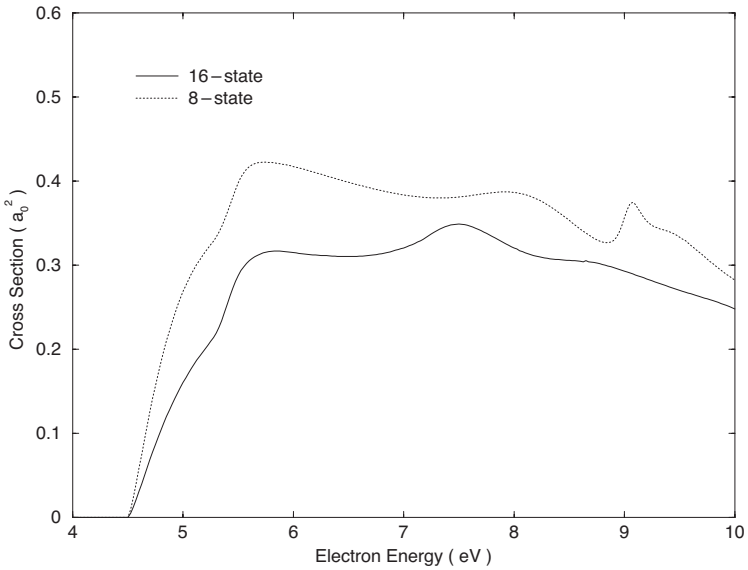

(*b*)

Figure 3. (*a*) Electron impact excitation of transition $X\,^1A_1$–$1\,^3B_1$ of Cl_2O. Solid curve: 16-state *R*-matrix cross sections; dotted curve: eight-state *R*-matrix cross section). (*b*) Electron impact excitation of transition $X\,^1A_1$–$1\,^3A_2$ of Cl_2O. Solid curve: 16-state *R*-matrix cross sections; dotted curve: eight-state *R*-matrix cross sections. (*c*) Electron impact excitation of transition $X\,^1A_1$–$1\,^3B_2$ of Cl_2O. Solid curve: 16-state *R*-matrix cross sections; dotted curve: eight-state *R*-matrix cross sections. (*d*) Electron impact excitation of transition $X\,^1A_1$–$1\,^3A_1$ of Cl_2O. Solid curve: 16-state *R*-matrix cross sections; dotted curve: eight-state *R*-matrix cross sections.

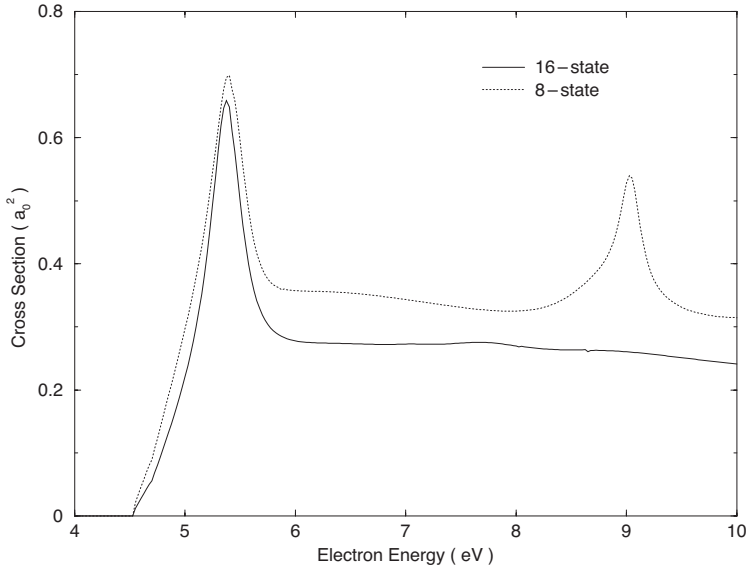

(*c*)

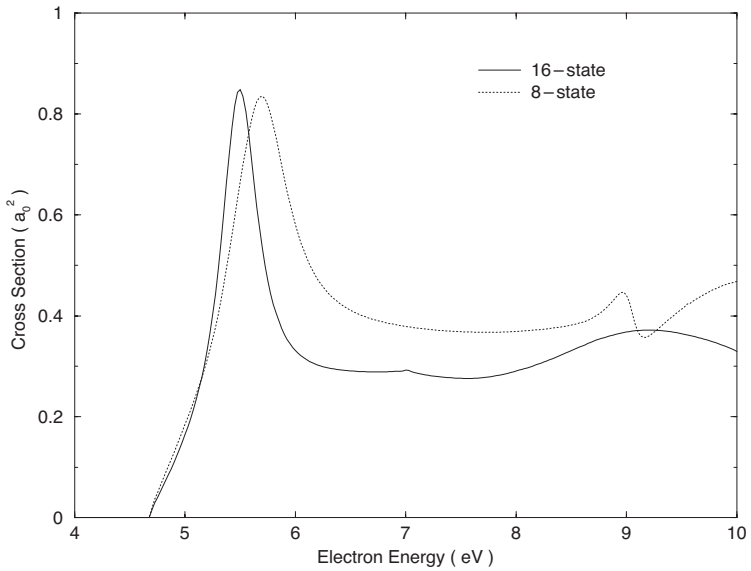

(*d*)

Figure 3. (Continued.)

symmetry at a higher energy around 9 eV. The dominating peak in the 16-state calculation is shifted to a lower energy with respect to the eight-state results. The pseudo-resonance structure is once again smoothed out when more channels are available for the loss of flux. The other symmetries contribute little or nothing to the cross sections just as in the nearby degenerate $^3B_2$ case.

Table 2 provides a summary of the various resonances found by our calculation. Attempts

Table 2. Symmetry, resonance position, resonance width, type of resonance and resonance assignment.

Symmetry	E_r (eV)	Γ_r (eV)	$E_r(L^2)$ (eV)	Assignment
$^2A_1$	5.590	0.464	5.82	$(2\,^3B_2)8b_2$
$^2A_1$	7.460	0.591	7.63	$(2\,^1B_2)8b_2$
$^2A_2$	5.261	0.550	5.26	$(2\,^3B_1)8b_2$
$^2A_2$	5.741	1.107	5.85	$(2\,^1B_1)8b_2$
$^2B_1$	3.679	0.202	3.53	$(2\,^3A_2)8b_2$
$^2B_1$	7.532	0.548	7.28	$(1\,^1A_2)8b_2$
$^2B_2$	2.096	0.971	2.44	$3b_1^2 8b_2$
$^2B_2$	5.383	0.487	5.76	$(2\,^3B_2)10a_1$

to assign these various resonances by manipulating the active space of our scattering calculation gave contradictory results. We therefore performed some 'bound state' calculations using only the target basis functions. In general, the results of such calculations for resonances need to be treated with caution (Stibbe and Tennyson 1999) but in the present case, presumably because of the lack of diffuse target functions, there was a one-to-one correspondence between the roots of the 'bound state' calculation and the resonances found in the scattering calculation. It is straightforward to determine the dominant configurations in the scattering calculations and these were used to assign the resonances, although some ambiguity remains as to whether the 'parent' electronic excited state is the singlet or the triplet. In practice both probably contribute. It is notable that, apart from the low-lying $^2B_2$ shape resonance discussed above, all the other resonances appear to be core-excited shape resonances rather than the Feshbach resonances one might have expected. These resonances are therefore all rather broad.

3.4. Variation with geometry

From the Cl_2O photolysis study (Nickolaisen *et al* 1996), the 1^1B_1 and 1^3A_2 states are believed to dissociate to products ClO and Cl. It is also known that the Cl–O bond in all the excited states considered here is either nonbonding or antibonding (Motte-Tollet *et al* 1998) and therefore these states are expected to be dissociative. Resonances can decay by autoionization or by dissociation into fragments through the process of dissociative electron attachment. Thus, the resonances have direct relevance to the study of low-energy dissociative electron attachment, which occurs when an electron is captured by a molecular target to form a temporary negative ion that subsequently dissociates into neutral and stable anion fragments. The dissociating anion states appear as resonances in the electron scattering cross section that may be observed in dissociative electron attachment channels in which one of the ions may be Cl^-, O^-, Cl_2^-, ClO^- or Cl_2O^-.

We have investigated the dependence of the shape resonance with respect to different geometries in C_{2v} and C_s symmetries. The A_1 and B_2 symmetries of the C_{2v} point group correlate with the A′ point group of C_s symmetry. We first studied the variation of the position and width of the shape resonance and the energies of the ground states of Cl_2O and Cl_2O^- for symmetric bending in C_{2v} symmetry. The bond length Cl–O is kept fixed at its equilibrium value of 3.2 a_0 and the bond angle is varied from 116° to 80°. As the bond angle decreases the shape resonance position moves to lower energies and the resonance becomes narrower up to a bond angle of 90°, beyond which the resonance position moves to higher energy and the width increases. This is summarized in table 3 where the energies of the ground states of Cl_2O and Cl_2O^- are relative to the ground-state energy of Cl_2O at the experimental equilibrium

Table 3. Variation of shape resonance and ground-state energies of Cl_2O and Cl_2O^- for symmetric bending in C_{2v} symmetry. All energies are with respect to the experimental equilibrium geometry of the ground state of Cl_2O at 110.9°.

Bond angle (deg)	E_r (eV)	Γ_r (eV)	Cl_2O (eV)	Cl_2O^- (eV)
116.0	2.349	1.025	0.0059	−0.5666
110.9	2.096	0.971	0.0000	−0.4423
106.0	1.939	0.915	0.0655	−0.3331
100.0	1.760	0.838	0.2666	−0.2267
95.0	1.658	0.788	0.5675	−0.1675
90.0	1.562	0.752	1.0310	−0.1428
80.0	1.628	0.825	2.6741	−0.1835

Table 4. Variation of shape resonance and ground-state energies of Cl_2O and Cl_2O^- for symmetric and asymmetric stretching at the experimental equilibrium bond angle. All energies are with respect to the experimental equilibrium geometry of the ground state of Cl_2O at $r_1 = r_2 = 2.096\ a_0$.

Bond lengths (r_1, r_2) (a_0)	E_r (eV)	Γ_r (eV)	Cl_2O (eV)	Cl_2O^- (eV)
(3.0, 3.0)	3.484	1.566	0.6503	0.3944
(3.1, 3.1)	2.776	1.257	0.2345	−0.0055
(3.2, 3.2)	2.096	0.971	0.0000	−0.4423
(3.3, 3.3)	1.488	0.707	−0.0991	−0.8762
(3.4, 3.4)	0.905	0.451	−0.0980	−1.2895
(3.1, 3.3)	2.579	1.176	0.0525	−0.4678

geometry. In table 4 we show some more results for symmetric and asymmetric stretches keeping the bond angle fixed at its experimental equilibrium value. We notice that as the Cl–O bonds are symmetrically stretched the shape resonance moves to lower energy and becomes narrower.

We also performed scattering calculations for different geometries in the C_s point group corresponding to stretching of one ClO bond while the other ClO bond remained fixed at its geometrical equilibrium value 3.2 a_0, with the bond angle also fixed at its equilibrium value. Figure 4 presents our results. As the stretching increases, the resonance position shifts to lower energies and it becomes narrower. As discussed previously (Baluja *et al* 2000), our method will overestimate anion energies at large internuclear separations because our diffuse functions are centred at the centre of mass rather than the atom which is carrying away the extra electron. Our calculations will therefore give a poor representation of anionic dissociation and crossing point between the shape resonance and the ground-state energy potential curve will be at too large a value. From symmetry considerations we infer that the shape resonance dissociates to the fragments $ClO(^2\Pi)$ state and $Cl^-(^1S)$ state.

3.5. Conclusions

This is the first study of theoretical electron impact on Cl_2O. It has provided a number of pointers to experimentalists, such as the presence of a low-lying $^2B_2$ shape resonance and a number of higher core-excited shape resonances. All of these resonances are found to be rather broad and will therefore be shortlived. Such resonances may be correlated with different dissociative attachment channels. Our calculations show the presence of an electronically bound anionic state of Cl_2O. However, this state appears to lie above the $ClO + Cl^-$ asymptote (Wecker *et al* 1981) and therefore it presumably lies on a dissociative potential.

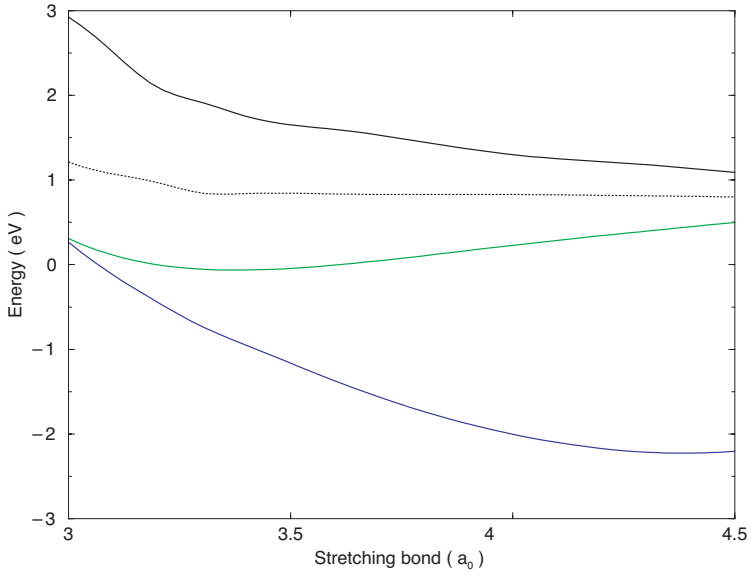

Figure 4. Shape resonance in C_s symmetry as a function of stretching one of the Cl–O bonds. Cl_2O^- anion ground state: lower dotted curve; anion excited state (shape resonance): upper dotted curve; shape resonance width: dot-dash curve; ground state of Cl_2O: solid curve.

Models developed in this paper are now being applied to the open-shell OClO molecule, for which some experimental results are available (Senn *et al* 1999, Field *et al* 2000).

Acknowledgment

This work was supported by the UK Engineering and Physical Sciences Research Council via a visiting Fellowship for KLB and other grants.

References

Baluja K L, Mason N J, Morgan L A and Tennyson J 2000 *J. Phys. B: At. Mol. Opt. Phys.* **33** L677
Beltrán A, Andrés J, Noury S and Silvi B 1999 *J. Phys. Chem.* A **103** 3078
Bru L, Perez Rodriguez M and Cubero M 1952 *J. Chem. Phys.* **20** 1069
Burke P G and Berrington K A (ed) 1993 *Atomic and Molecular Processes: an R-Matrix Approach* (Bristol: Institute of Physics Publishing)
Cornford A B, Frost D C, Herring F G and McDowell C A 1971 *J. Chem. Phys.* **55** 2820
Crawford O H and Dalgarno A 1971 *J. Phys. B: At. Mol. Phys.* **13** 494
Crawford O H and Garrett W R 1977 *J. Chem. Phys.* **66** 4968
Del Bene J E, Watts J D and Bartlett R J 1995 *Chem. Phys. Lett.* **246** 541
Dunitz J D and Hedberg K 1950 *J. Chem. Soc.* **72** 3108
Dunning T H and Hay P J 1977 *Methods of Electronic Structure Theory* vol 2, ed H F Schaefer (New York: Plenum)
Fabrikant I I 1977 *J. Phys. B: At. Mol. Phys.* **10** 1761
Field D, Jones N C, Gingell J M, Mason N J, Lunt S L and Ziesel J P 2000 *J. Phys. B: At. Mol. Opt. Phys.* **33** 1039
Finkelnburg W, Schumacher H J and Stieger G 1931 *Z. Phys. Chem.* **15** 127
Gianturco F A and Jain A 1986 *Phys. Rep.* **143** 347
Goodeve C F and Wallace J I 1930 *Trans. Faraday Soc.* **26** 254
Hariharan P C and Pople J A 1973 *Theor. Chim. Acta* **28** 213
Herberich G E, Jackson R H and Millen D J 1966 *J. Chem. Soc.* A 336
Knauth H D, Alberti H and Clausen H 1979 *J. Phys. Chem.* **83** 1604

Lee T J 1996 *J. Phys. Chem.* **99** 15074
Lin C L 1976 *J. Chem. Eng. Data* **21** 411
Magnusson E and Schaefer H F 1985 *J. Chem. Phys.* **83** 5721
McGrath M P, Clemitshaw K C, Rowland F S and Hehre W J 1990 *J. Phys. Chem.* **94** 6126
Molina L T and Molina M J 1978 *J. Phys. Chem.* **82** 2410
Morgan L A 1998 *J. Phys. B: At. Mol. Opt. Phys.* **31** 5003
Morgan L A, Gillan C J, Tennyson J and Chen X 1997 *J. Phys. B: At. Mol. Opt. Phys.* **30** 4087
Morgan, L A, Tennyson J and Gillan C J 1998 *Comput. Phys. Commun.* **114** 120
Motte-Tollet F, Delwiche J, Heinesch J, Hubin-Franskin M J, Gingell J M, Jones N C, Mason N J and Marston G 1998 *Chem. Phys. Lett.* **284** 452
Motte-Tollet F, Ska M P, Marston G M, Walker I C, Siggel M R F, Gingell J M, Kaminski L, Brown K and Mason N J 1997 *Chem. Phys. Lett.* **275** 298
Nakata M, Sugic M, Takeo H, Matsumura C, Fukuyama and Kuchitsu K 1981 *J. Mol. Spectrosc.* **86** 241
Nee J B 1991 *J. Quant. Spectrosc. Radiat. Transfer* **46** 55
Nickolaisen S L, Miller C E, Sander S P, Hand M R, Williams I H and Francisco J S 1996 *J. Chem. Phys.* **104** 2857
Sailer W, Tegeder P, Drexel H, Mason N J, Meinke M, Illenberger E and Mark T D 2001 *Chem. Phys. Lett.* at press
Sarpal B K, Branchett S E, Tennyson J and Morgan L A 1991 *J. Phys. B: At. Mol. Opt. Phys.* **24** 3685
Sarpal B K, Pfingst K, Nestmann B M and Peyerimhoff S D 1996 *J. Phys. B: At. Mol. Opt. Phys.* **29** 857
Senn G, Drexel H, Marston G, Mason N J, Mark T D, Meinke M, Schmale C, Tegeder P, Ruhl E and Illenberger E 1999 *J. Phys. B: At. Mol. Opt. Phys.* **32** 3615
Stibbe D T and Tennyson J 1999 *Chem. Phys. Lett.* **308** 532–6
Tennyson J 1996a *J. Phys. B: At. Mol. Opt. Phys.* **29** 1817
——1996b *J. Phys. B: At. Mol. Opt. Phys.* **29** 6185
Tennyson J and Noble C J 1984 *Comput. Phys. Commun.* **32** 421
Toniolo A, Persico M and Pitea D 2000 *J. Phys. Chem.* A **31** 7278
Wecker D, Christodoulides A A and Schindler R N 1981 *Int. J. Mass Spectrom. Ion Phys.* **38** 391